Postbiotic metabolites from *Bifidobacterium adolescentis* alleviates doxorubicin-induced aging in canine vascular endothelial cells

HONGCHEN JIN[1], HUASONG BAI[1], TONG LIU[1], HENGYAN WANG[1], YUNLIANG LI[2] and ZHANZHONG WANG[3]

[1]Nourse Science Centre for Pet Nutrition, Wuhu, Anhui 241200, P.R. China; [2]School of Food and Biological Engineering, Jiangsu University, Zhenjiang, Jiangsu 212013, P.R. China; [3]School of Synthetic Biology and Biomanufacturing, Tianjin University, Tianjin 300072, P.R. China

Received December 18, 2025; Accepted April 27, 2026

DOI: 10.3892/etm.2026.13218

Abstract. Cardiovascular aging represents the initial stage of systemic bodily aging. Endothelial cell (EC) senescence serves a key role in vascular aging. However, therapeutic strategies targeting ECs senescence remain insufficiently explored. The present study aimed to assess the anti-aging effects of metabolites derived from brown algae extract fermented by *Bifidobacterium adolescentis* Life Age 20-k9 (LA20k9) based on a canine vascular endothelial cell (CVEC) model and elucidate its underlying cellular mechanisms. Results showed that LA20k9 was able to promote the proliferation of CVECs. LA20k9 also significantly reduced aging-related β-galactosidase activity, which decreased by 30% compared with the doxorubicin-induced aging group. LA20k9 treatment exerted anti-aging effects and improved vascular health, as evidenced by decreased levels of MMPs (including MMP-1 and MMP-3) and increased VEGF and basic fibroblast growth factor contents. LA20k9 treatment significantly reduced oxidative stress and inflammatory responses in CVECs, as evidenced by decreased levels of inflammatory factors and malondialdehyde and increased NAD^+, superoxide dismutase and glutathione content. Mechanistically, LA20k9 activated the cell cycle system, cAMP signaling pathway and retinol metabolism whilst inhibiting cellular senescence, oxidative damage and inflammatory responses that ameliorate vascular aging. Collectively, these findings identified LA20k9 as a promising metabolite that can be used in a postbiotic strategy to counteract vascular aging and promote healthy longevity.

Correspondence to: Professor Zhanzhong Wang, School of Synthetic Biology and Biomanufacturing, Tianjin University, 92 Weijin Road, Tianjin 300072, P.R. China
E-mail: wzz7698@tju.edu.cn

Abbreviation: LA20k9, Life Age 20k9

Key words: Bifidobacterium adolescentis, postbiotic metabolites, anti-vascular aging, transcriptomics, metabolomics

Introduction

Aging, as a natural law associated with the degenerative functional and organic process that occurs in the body with age, can lead to and aggravate degenerative diseases (1-3). Studies have shown that aging markedly increases the incidence of cardiovascular diseases (CVDs) such as myocardial ischemia, atherosclerosis and cardiac fibrosis (4-7). Oxidative stress is a key factor in cardiac aging, while the inflammatory response is an important defense mechanism of the heart; both can affect the structure of myocardial cells and cardiac function (8). Cellular senescence is a core mechanism of organismal aging. It has received in-depth attention in recent years due to its pathological importance as a driving factor of chronic diseases (9). Endothelial cell (ECs) senescence serves a key role in the process of vascular aging. ECs dysfunction is directly involved in processes such as the formation of atherosclerotic plaques, the decrease in vascular elasticity and the pathological remodeling of hypertension (10-12). These previous studies emphasized that cellular senescence is not only a sign of organismal aging but also a driving factor for numerous chronic diseases (13-15). Senescent ECs exhibit the characteristics of mitochondrial dynamic imbalance, which directly affects the structure and function of blood vessels and thereby promotes the development of CVDs (16). Therefore, seeking effective strategies to intervene in ECs senescence is of great importance for delaying blood vessel aging and the progression of associated diseases.

Probiotic cultures that have undergone inactivation treatment are collectively referred to as postbiotics (17). In a broad sense, the concept of postbiotics encompasses both bacteria and their metabolic products, which possess biological activities similar to or better than those of live bacteria, such as antibacterial, antioxidant, anti-inflammatory and immunomodulatory properties (18).

Bifidobacterium is widely present in the intestines of humans and animals. It exerts regulatory effects on the brain-gut axis and can be used to treat irritable bowel

syndrome, alleviate depression and improve cognitive impairment. Its probiotic properties can be used to relieve immune-associated diseases such as allergies and colitis (19). However, research on *Bifidobacterium* and the regulation of cardiovascular health by its metabolites is still relatively scarce. Previously, a strain of *Bifidobacterium adolescentis* Life Age 20 was isolated from the feces of long-lived cats (20). A mouse experiment further demonstrated that this strain could markedly extend the lifespan of mice with accelerated aging (20). Based on this result, an additional strain of *Bifidobacterium adolescentis*, Life Age 20k9 (LA20k9), was isolated preserved in the China Center for Type Culture Collection (preservation no. CCTCC-M-025638), from the feces of long-lived dogs. The aim of the present study was to investigate the anti-aging effects of the fermentation products of *Bifidobacterium adolescentis* in brown algae extract on canine blood vessels and explore its potential mechanism.

In the present study, an *in vitro* canine vascular endothelial cell (CVEC) model was employed to investigate the anti-vascular aging effects of LA20k9. The effects of LA20k9 on vascular senescence, endothelial function, inflammation and the molecular markers of aging were assessed to establish an association between treatment response and cellular aging status. Transcriptomics and metabolomics are widely employed high-throughput omics approaches in biological research (21,22). Transcriptomic profiling enables the systematic quantification of gene expression dynamics across experimental conditions, whereas metabolomic profiling captures condition-dependent alterations in small-molecule metabolite abundances. Integrating this complementary molecular information affords a more holistic view of biological system responses, thereby enhancing mechanistic insight in biomedical and translational research. Accordingly, transcriptomic and metabolomic analyses were jointly applied to comprehensively elucidate the molecular mechanisms underlying the observed biological activities. The present study aimed to assess the anti-aging effects of metabolites derived from brown algae extract fermented by LA20k9 based on a CVEC model and elucidate its underlying cellular mechanisms. The present findings could provide both scientific and practical implications for the potential therapeutic applications of LA20k9, supporting the development of novel biological interventions targeting post-aging processes.

Materials and methods

Reagents and materials. A *Bifidobacterium adolescentis* LA20k9 strain was isolated from the feces of an elderly dog (accession no: CCTCC-M-2025638). For LA20k9 fermentation and freeze-drying, the seed culture of *Bifidobacterium adolescentis* LA20k9, preserved in 15% glycerol (Oxoid; Thermo Fisher Scientific, Inc.), was inoculated into De Man-Rogosa-Sharpe medium (Oxoid; Thermo Fisher Scientific, Inc.) containing 2% (v/v) brown algae extract (derived from *Laminaria japonica*; Shanxi Benhe Biotechnology Engineering Co., Ltd.) and anaerobic culture was carried out at 38˚C for 48 h.

Furthermore, 15% glycerol without *Bifidobacterium adolescentis* LA20k9 was fermented under the same conditions, with blank substrate fermentation metabolite (BMFM) excluding LA20-k9. The supernatant of the fermentation broth was collected after room temperature centrifugation for 10 min at 2,000 x g and freeze-dried. CVECs [Global Pet Cell Resource Center (PETCC)-199 cell line; cat. no. PETCC#199] were obtained from the PETCC (Tianjin, China). Doxorubicin (DOX) was purchased from Shanghai Aladdin Biochemical Technology Co., Ltd. Hanks' balanced salt solution (HBSS), the senescence-associated β-galactosidase (SA-β-gal) staining kit and SA-β-gal activity assay kit were purchased from Beijing Solarbio Science & Technology Co., Ltd. Trypsin, FBS, TRIzol® and M-3 medium were obtained from Gibco (Thermo Fisher Scientific, Inc.). Canine ELISA kits for MMP-1 (cat. no. ml031816), MMP-3 (cat. no. ml024650), VEGF (cat. no. ml031966), basic fibroblast growth factor (bFGF; cat. no. ml031890), granulocyte-macrophage colony stimulating factor (GM-CSF; cat. no. ml002650) and inflammatory factors IL-1β (cat. no. ml024767), TNF-α (cat. no. ml031931), IL-6 (cat. no. ml024780), IL-8 (cat. no. ml024786) and monocyte chemotactic protein-1 (MCP-1; cat. no. ml002710) were obtained from Shanghai Enzyme-linked Biotechnology Co., Ltd. Oxidative stress-associated kits for superoxide dismutase (SOD; cat. no. S0101S), malondialdehyde (MDA; cat. no. S0131S) and glutathione (GSH; cat. no. S0053).

Analysis of the composition of LA20k9 and BMFM

Detection of monosaccharide and polysaccharide contents. Disaccharide and monosaccharide contents of LA20k9 and BMFM were determined using precolumn derivatization with 1-phenyl-3-methyl-5-pyrazolone (PMP) (cat. no. A501894-0250; Sangon Biotech Co., Ltd.) and high-performance liquid chromatography (HPLC). LA20k9 and BMFM were hydrolyzed in 10 ml 7.2% sulfuric acid (cat. no. S962529; Shanghai Macklin Biochemical Co., Ltd.) under nitrogen at 110˚C for 2 h. After hydrolysis, 0.5 ml the sample was neutralized and diluted with water to 1 ml. Monosaccharide standards [glucose (cat. no. D823520) and fucose (cat. no. L809666) were obtained from Shanghai Macklin Biochemical Co., Ltd.] or hydrolyzed LA20k9 and BMFM were derivatized with 0.2 ml 0.3 M sodium hydroxide (cat. no. R885161; Shanghai Macklin Biochemical Co., Ltd.) and 0.4 ml PMP solution. The mixture was incubated at 70˚C for 60 min under nitrogen. Afterward, 0.2 ml 0.3 M hydrochloric acid (cat. no. C0680110271; Nanjing Chemical Reagent Co., Ltd.) was added and the volume was adjusted to 2 ml with water. Chloroform (1.5 ml; cat. no. C1481519267; Nanjing Chemical Reagent Co., Ltd.) was added, shaken and the organic layer discarded. The aqueous phase was filtered through a 0.45 μm aqueous membrane and analyzed on an Agilent 1200 HPLC system (Agilent Technologies, Inc.) with a C18 (250.0x4.6 mm; 5 μm) column and UV detection. The method of monosaccharide concentration detection followed the same procedure as described for polysaccharide content analysis, excluding the hydrolysis step.

Protein content. LA20k9 and BMFM protein content was determined using the Pierce™ BCA protein assay kit (cat. no. A65453; Thermo Fisher Scientific, Inc.). A 20 mg sample was accurately weighed and dissolved in 1 ml ultrapure water, followed by a 200-fold dilution to prepare the sample solution. Then, 20 μl solution was mixed with 200 μl BCA working reagent. The reaction mixture was incubated at 37˚C for

30 min and the absorbance at 562 nm was measured at the end of the incubation.

Detection of amino acid content. LA20k9 and BMFM amino acid content was determined by HPLC coupled with pre-column derivatization using o-phthaldialdehyde (OPA) (cat. no. 26025; Thermo Fisher Scientific, Inc.). LA20k9 and BMFM were hydrolyzed in 10 ml 6 M hydrochloric acid under nitrogen at 110˚C for 24 h to prevent oxidation. After hydrolysis, 100 μl sample solution or amino acid standard [aspartic acid (cat. no. L708685), threonine (cat. no. H818497), serine (cat. no. D794545), glutamic acid (cat. no. D665473), glycine (cat. no. G800880), alanine (cat. no. D688836), cystine (cat. no. D804429), valine (cat. no. V828207), methionine (cat. no. L675564), isoleucine (cat. no. H811900), leucine (cat. no. D688815), tyrosine (cat. no. D818619), phenylalanine (cat. no. D793640), histidine (cat. no. D810956), lysine (cat. no. D856989), arginine (cat. no. H677986) and proline (cat. no. D794397) obtained from Shanghai Macklin Biochemical Co., Ltd.] was mixed with 200 μl OPA reagent. The mixture was vortexed vigorously for 30 sec and allowed to react at room temperature in the dark for 15-20 min. After reaction, the mixture was filtered through a 0.22 μm aqueous membrane to remove particulates prior to HPLC analysis. HPLC separation was performed on an Agilent 1200 HPLC system (Agilent Technologies, Inc.) equipped with a C18 reversed-phase column. The mobile phase consisted of 0.1 M PBS (pH 8.0; solvent A) and a mixture of methanol (cat. no. C0690110124; Nanjing Chemical Reagent Co., Ltd.) and acetonitrile [cat. no. C0560116005; Nanjing Chemical Reagent Co., Ltd.; 1:1 (v/v) solvent B]. A linear gradient elution was employed as follows: 0-10 min, 10-30% B; 10-25 min, 30-50% B; 25-30 min, 50-10% B; and 30-35 min, 10% B for equilibration. The flow rate was set at 1.0 ml/min and the column temperature was maintained at 30˚C. Amino acids were emission wavelengths set at 340 and 450 nm, respectively.

Detection of organic acid content. Organic acid content was determined by HPLC. The analysis was performed on a reversed-phase C18 column with 0.01 mol/l potassium dihydrogen phosphate solution (pH 2.5-3.0; cat. no. P837011; Shanghai Macklin Biochemical Co., Ltd.) as the mobile phase at a flow rate of 1.0 ml/min. The column temperature was maintained at 30˚C and the detection wavelength was set at 210 nm. The injection volume was 20 μl. Samples or organic acid standard [tartaric acid (cat. no. D666102), malic acid (cat. no. D689340), lactic acid (cat. no. D742481), pyruvic acid (cat. no. P796878), oxalic acid (cat. no. S818087), acetic acid (cat. no. A801299), citric acid (cat. no. C805019), succinic acid (cat. no. S874398), propionic acid (cat. no. P757623) and benzenolactic acid (cat. no. L795422) obtained from Shanghai Macklin Biochemical Co., Ltd.] were dissolved in water, vortexed to mix, prepared as standard working solutions at room temperature and filtered through a 0.22 μm aqueous membrane before injection. Quantification was carried out using the external standard method (23,24). Calibration curves were constructed by plotting peak areas against corresponding standard concentrations. The contents of individual organic acids in samples were calculated based on the calibration equations.

Cell culture. CVECs were authenticated by the supplier and tested negative for *Mycoplasma* contamination. The cells were cultured in modified M3-DMEM medium (PETCC) supplemented with 12% FBS. Cultures were maintained in an atmosphere humidified with 5% CO_2 until 90% confluence before use.

Cell viability assay. Cell viability was assessed using a Cell Counting Kit-8 (CCK-8) assay (Beyotime Biotechnology). CVECs were stained with trypan blue at room temperature for 5 min, counted and adjusted to $1x10^4$ cells/ml. The cells were seeded into 96-well plates and incubated for 24 h at 37˚C with numerous concentrations of LA20k9 (0, 20, 40, 80, 160, 320, 640 and 1,280 μg/ml), BMFM (0, 20, 40, 80, 160, 320, 640 and 1,280 μg/ml) and DOX (0, 0.2, 0.3, 0.4, 0.5, 0.6, 0.7, 0.8, 0.9 and 1.0 μmol/l). After removing the drug solutions, 110 μl HBSS containing 10% CCK-8 was added, mixed for 30 sec and incubated for 2 h. Absorbance was then measured at 450 nm. HBSS without drugs served as the negative control (NC). DOX at 60-70% viability was used to induce senescence.

The following groups were established to assess the capacity of LA20k9 and BMFM to restore the viability of DOX-induced vascular ECs: HBSS with only DOX (senescence model group); DOX with varying concentrations of LA20k9 (LA20k9 treatment groups); DOX with varying concentrations of BMFM (BMFM treatment groups); and HBSS alone (NC group). The procedures were the same as those used to determine the drug concentrations.

SA-β-gal activity assay. CVECs were seeded in 6-well plates at a density of $1x10^6$ cells/well and cultured at 37˚C and 5% CO_2 for 24 h until the cells adhered. Drug treatment groups were the same as those used for the cell viability assay. After 24 h, quantitative and qualitative analyses were conducted using the SA-β-gal activity detection kit and the SA-β-gal staining kit, respectively, following the manufacturer's protocols.

Evaluation of cellular senescence markers. CVECs were seeded in 6-well plates at a density of $1x10^6$ cells/well and cultured at 37˚C and 5% CO_2 for 24 h until the cells adhered. Drug treatment groups were the same as those used in the cell viability assay. After 24 h, the levels of MMP-1, MMP-3, VEGF, bFGF, IL-1β, TNF-α, IL-6, IL-8, GM-CSF and MCP-1 were measured using ELISA kits. Canine ELISA kits for MMP-1 (cat. no. ml031816), MMP-3 (cat. no. ml024650), VEGF (cat. no. ml031966), basic fibroblast growth factor (bFGF; cat. no. ml031890), granulocyte-macrophage colony stimulating factor (GM-CSF; cat. no. ml002650) and inflammatory factors IL-1β (cat. no. ml024767), TNF-α (cat. no. ml031931), IL-6 (cat. no. ml024780), IL-8 (cat. no. ml024786) and monocyte chemotactic protein-1 (MCP-1; cat. no. ml002710) were obtained from Shanghai Enzyme-linked Biotechnology Co., Ltd. Specifically, 50 μl supernatant from each treatment group was added to wells pre-coated with primary antibodies specific to either canine protein. HRP-conjugated secondary antibodies were then added and the plates were incubated at 37˚C for 60 min. After incubation, the wells were washed five times with PBS with Tween 20, followed by the addition of 100 μl 3,3',5,5'-tetramethylbenzidine substrate for color development. Absorbance was measured at 450 nm.

Evaluation of oxidative stress markers. CVECs were seeded in 6-well plates at a density of $1x10^6$ cells/well and cultured at 37˚C and 5% CO_2 for 24 h until the cells adhered. The treatment groups were the same as used for the cell viability assay. After 24 h of action, the SOD content was detected using a total SOD activity detection kit, following the manufacturer's protocols and absorbance was measured at 450 nm. MDA content was used to assess lipid oxidation levels. MDA was measured in cell lysates using a colorimetric lipid oxidation detection kit, following the manufacturer's protocols. Absorbance was measured at 532 nm. GSH content was measured using a GSH detection kit, following the manufacturer's protocols. GSH levels were measured by mixing 20 μl sample with 5,5'-dithiobis (2-nitrobenzoic acid) solution, allowing the reaction to proceed for 5 min and reading the absorbance at 405 nm. An enhanced NAD^+ detection kit was used to measure the NAD^+ content through sequential incubation with ethanol dehydrogenase, followed by the addition of a colorimetric reagent in strict accordance with the manufacturer's instructions. Protein concentrations were quantified using a BCA kit (Thermo Fisher Scientific, Inc.).

RNA sequencing. Cells from different treatment groups were lysed using TRIzol reagent. Phase separation was achieved by adding chloroform, followed by RNA precipitation with isopropanol and washing with ethanol. The isolated RNA was dissolved in RNase-free water (cat. no. R0022; Beyotime Biotechnology). RNA concentration and integrity were verified using an Agilent 5400 Bioanalyzer (Agilent Technologies, Inc.). mRNA was enriched using Oligo(dT) beads and fragmented in a buffer with divalent cations [NEBNext® Poly(A) mRNA Magnetic Isolation Module; cat. no. E7490; New England Biolabs, Inc.]. First-strand cDNA was synthesized using Moloney Murine Leukemia Virus Reverse Transcriptase (New England Biolabs, Inc.), followed by second-strand synthesis with DNA polymerase I and RNase H (NEBNext® Ultra™ II RNA Library Prep; cat. no. E7775L; New England Biolabs, Inc.). The double-stranded cDNA underwent end repair, A-tailing, adaptor ligation and AMPure XP bead purification, then PCR amplification to construct the cDNA library (NEBNext® Ultra™ II RNA Library Prep; cat. no. E7775L; New England Biolabs, Inc.). The sequencing was carried out using the NovaSeq 6000 platform (Illumina, Inc.) employing a paired-end 150 bp approach. The final loading concentration of the library was 1.5 μg/μl.

To generate clean data, sequencing reads were filtered to remove adapters, ambiguous bases and low-quality sequences. The filtered reads were aligned to the reference genome with Hierarchical Indexing for Spliced Alignment of Transcripts (version 2.2.1; https://daehwankimlab.github.io/hisat2/download/). Gene expression quantification was performed using featureCounts (version 2.0.6; https://subread.sourceforge.net/featureCounts.html) to tally reads mapped to each gene, with results expressed as fragments per kilobase of transcript per million (FPKM) mapped reads. Principal component analysis was applied to the FPKM values. Differential expression was analyzed using the 'DESeq2' package (version 1.42.0; R software; Posit Software, PBC; https://bioconductor.org/packages//release/bioc/html/DESeq2.html). Raw read count data were normalized to correct for sequencing depth differences. Statistical models calculated P-values for each gene, which were adjusted for multiple testing using the Benjamini-Hochberg method to obtain adjusted P-values. Differentially expressed genes (DEGs) were identified based on a fold change of ≥1.2 and adjusted P≤0.05. Normalization and hierarchical clustering of DEGs' FPKM expression matrices were performed using the 'ggplot2' package in R software (version 3.0.3; Posit Software, PBC; https://ggplot2.tidyverse.org/), with heatmap clustering conducted using the 'pheatmap' package (https://cran.r-project.org/web/packages/pheatmap/index.html).

To determine impacted signaling pathways and biological processes, Gene Set Enrichment Analysis (GSEA) was conducted using Gene Ontology (GO; https://www.geneontology.org/) and Kyoto Encyclopedia of Genes and Genomes (KEGG). Genes were ranked by differential expression between groups using 'Signal2Noise' as the ranking metric. Enrichment scores for each gene set were calculated using permutation tests and normalized enrichment scores were obtained to account for gene set size. Significance was assessed by computing P-values and false discovery rates (FDR), with FDR <0.25 indicating significant enrichment. The EnrichmentMap tool (version 3.3.1; https://apps.cytoscape.org/apps/enrichmentmap) was used to visualize GSEA results.

Non-targeted metabolome analysis. Untargeted metabolomic profiling was performed to investigate treatment-related metabolic alterations in CVECs. After treatment, CVECs were digested with trypsin for 2 min at 37˚C and then neutralized with PBS. Cell pellets were obtained by centrifuging at 1,000 x g for 5 min (at 4˚C; 5702 R centrifuge; Eppendorf SE). Samples were sent to Novogene Co., Ltd. for analysis using a liquid chromatography-tandem mass spectroscopy platform (Thermo Fisher Scientific, Inc.).

Statistical analysis. All data are expressed as the mean ± SD. Each group contained ≥4 replicates and CCK-8 assays were performed with a minimum of 12 replicates per condition. Statistical analyses were conducted using SPSS software (version 26.0; IBM Corp.). One-way ANOVA followed by Least Significant Difference or Games-Howell post-hoc tests was used for the datasets. The linear correlation between the transcriptome analysis samples was assessed by Pearson's correlation analysis and the correlation coefficient (r) was calculated. P-values were calculated using unpaired t-test. P<0.05 was considered to indicate a statistically significant difference.

Results

Identification of the composition of LA20k9. Components of LA20k9 and BMFM were analyzed (Table SI). The most significant difference between the two was in the organic acid component. LA20k9 contained 26.63 mg/g of malic acid and 59.17 mg/g of succinic acid, while these two organic acids were absent in BMFM. These two metabolites are the main biologically active metabolites produced by LA20k9. Malic acid and succinic acid are used in anti-aging studies due to their excellent performance in repairing oxidative damage and anti-inflammatory activity (25,26). Therefore, the results suggest that LA20k9 has anti-aging effects.

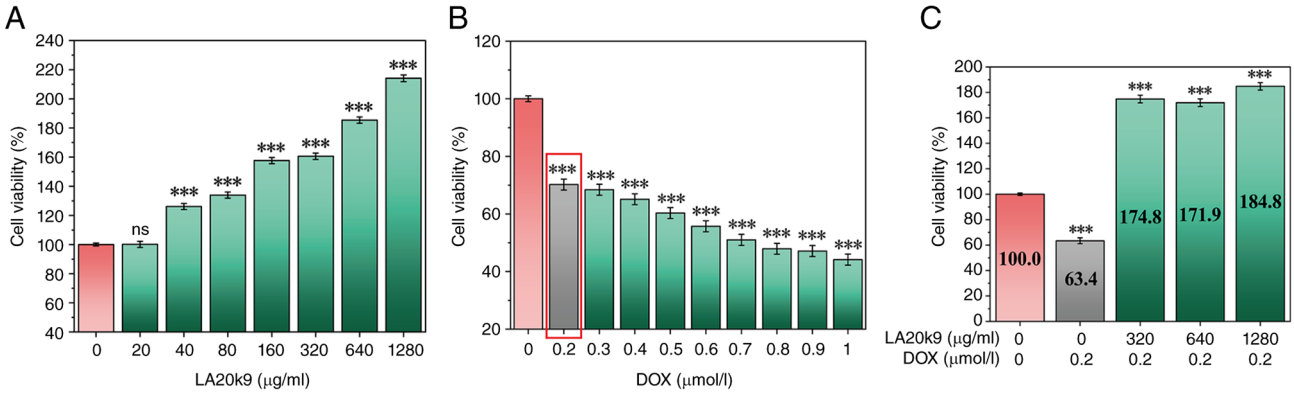

Figure 1. Effects of *Bifidobacterium adolescentis* LA20k9 fermentation metabolites on cell viability in CVECs. (A) Cell viability of CVECs treated with varying concentrations of LA20k9 (20-1,280 μg/ml). (B) Cell viability of CVECs treated with varying concentrations of DOX (0-1.0 μmol/l). (C) Cell viability of CVECs treated with LA20k9 (320, 640 and 1,280 μg/ml) in the presence of DOX (0.2 μmol/l). Cell viability assays were performed with at least 12 replicates per group. Data are presented as the mean values with error bars representing SD. P-values indicate specific comparisons between the indicated groups. ***P<0.001. LA20k9, Life Age 20k9; CVEC, canine vascular endothelial cells; DOX, doxorubicin.

Viability of canine vascular endothelial cells. Fig. 1A shows the cell viability after LA20k9 treatment. The three concentrations with the highest cell survival rates (320, 640 and 1,280 μg/ml) were selected for subsequent experiments. As shown in Fig. S1A, for BMFM, concentrations of 160, 320 and 640 μg/ml were utilized for comparative analysis.

The effects of different DOX concentrations (0-1.0 μmol/l) on cell viability were evaluated to determine the optimal concentration for inducing aging. With increases in DOX concentration, the viability of CVECs gradually decreased, demonstrating DOX dose-dependency (Fig. 1B). A DOX concentration of 0.2 μmol/l significantly reduced cell viability to 70.2% (P<0.05) and was selected as the concentration for DOX-induced CVEC senescence.

After adding 320, 640 and 1,280 μg/ml LA20k9 to 0.2 μmol/l DOX, the viability of CVECs increased to varying degrees (Fig. 1C). Among them, 1280 μg/ml LA20k9 most significantly improved cell viability (P<0.05), which was be restored to 184.8%, markedly exceeding the level of the NC group. As shown in Fig. S1B, after adding 320 μg/ml BMFM to 0.2 μmol/l DOX, the cell viability of CVEC showed the most significant improvement, reaching 90.7% (P<0.05). Notably, the regenerative capacity of LA20k9 markedly surpassed that of the BMFM. This performance gap suggests that the bioactive potency was not inherent to the raw algal substrate but was specifically generated through *B. adolescentis* fermentation. Therefore, subsequent experiments were conducted at 0.2 μmol/l DOX + 1,280 μg/ml LA20k9 and 0.2 μmol/l DOX + 640 μg/ml BMFM.

Effect of LA20k9 on the activity of SA-β-gal in CVECs. SA-β-gal accumulates in lysosomes and has become a commonly used biomarker for identifying senescent cells (27,28). After treating CVECs with DOX for 24 h, the SA-β-gal activity significantly increased by 16% compared with the control group (P<0.05) and the number of blue-infiltrated senescent cells also increased (Fig. 2A and B). After treatment with 1280 μg/ml LA20k9, SA-β-gal activity was significantly reduced by 16% (P<0.05) and the number of blue-infiltrated senescent cells was also decreased.

By contrast, BMFM failed to mitigate this response, exhibiting activity levels statistically indistinguishable from the DOX model group. This quantitative profile was visually corroborated by microscopic imaging (Fig. 2B). These results indicated that the anti-aging effect was not derived from the non-fermented algae extract itself but was specifically produced through the fermentation process of *Bifidobacterium adolescentis*.

Effect of LA20k9 on the levels of senescence-associated secretory phenotype (SASP) markers in CVECs. SASP markers represent the hallmark features of cellular senescence, influencing intercellular communication through paracrine signaling within the tissue microenvironment and thereby contributing to diverse physiological and pathological outcomes (29-32). The expression levels of SASP markers, including MMP-1, MMP-3, VEGF and bFGF, were evaluated in CVECs to assess the impact of LA20k9 on DOX-induced senescence.

DOX treatment significantly increased the levels of MMP-1 and MMP-3 and significantly reduced VEGF and bFGF content (P<0.05; Fig. 3). However, MMP-1 and MMP-3 levels significantly decreased after LA20k9 treatment, while VEGF and bFGF content significantly increased (P<0.001). Specifically, MMP-1 levels increased from 53.4 ng/ml (NC) to 80.5 ng/ml (DOX) and decreased to 52.8 ng/ml with DOX + LA20k9 treatment. MMP-3 levels increased from 21.0 ng/ml (NC) to 26.6 ng/ml (DOX) and decreased to 24.8 ng/ml with DOX + LA20k9 treatment. VEGF levels decreased from 132.9 pg/ml (NC) to 102.6 pg/ml (DOX) and increased to 129.6 pg/ml with DOX + LA20k9 treatment. bFGF levels decreased from 23.7 pg/ml (NC) to 20.8 pg/ml (DOX) and increased to 31.4 pg/ml with DOX + LA20k9 treatment. These results indicated that LA20k9 protected the structure and function of vascular ECs under senescence conditions by inhibiting the expression of MMP-1 and MMP-3 and upregulating the expression of VEGF and bFGF in CVECs, thereby preventing DOX-induced ECM degradation and the renewal of senescent cells.

Effect of LA20k9 on the levels of inflammatory response and oxidative stress response in CVECs. NAD^+ is a central coenzyme in cells that participates in energy metabolism, redox

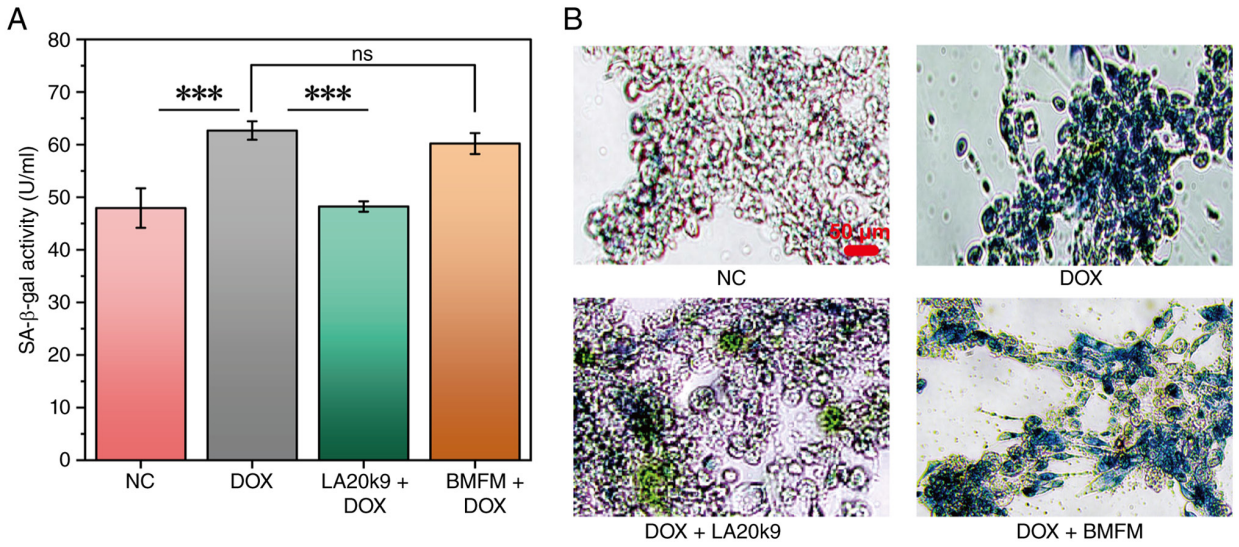

Figure 2. Effects of LA20k9 and BMFM on SA-β-gal activity in CVECs. Quantification (A) and representative images (B) showing SA-β-gal staining in CVEC with DOX-induced senescence. CVECs were treated with 0.2 μmol/l DOX and 1,280 μg/ml LA20k9 or 0.2 μmol/l DOX and 640 μg/ml BMFM. SA-β-gal activity assays were conducted with at least four replicates per group. Data are presented as the mean values with error bars representing SD. ***P<0.001. Scale bar, 50 μm. LA20k9, Life Age 20k9; BMFM, blank substrate fermentation metabolite; CVEC, canine vascular endothelial cells; SA-β-gal, senescence-associated β-galactosidase; DOX, doxorubicin; NC, negative control.

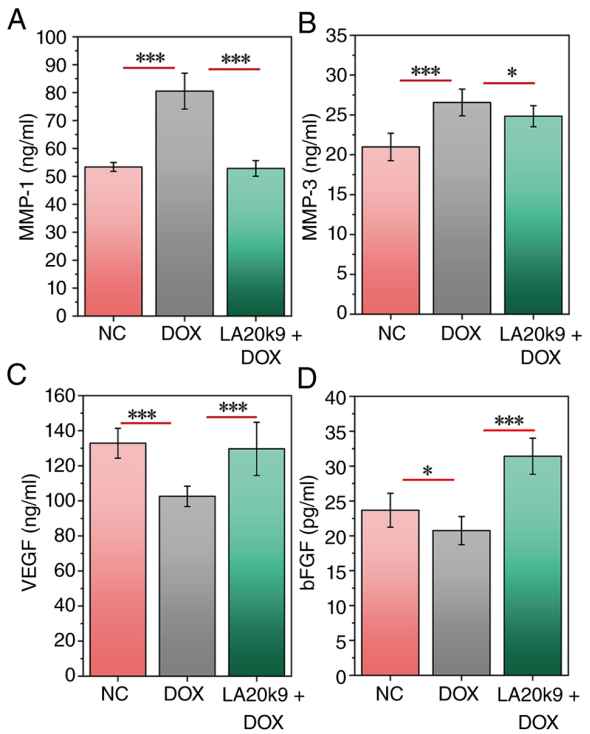

Figure 3. Effects of LA20k9 on SASP in CVECs. Levels of (A) MMP-1, (B) MMP-3, (C) VEGF and (D) bFGF in CVECs with DOX-induced senescence. CVECs were treated with 0.2 μmol/l DOX and 1,280 μg/ml LA20k9. SASP assays were conducted with at least four replicates per group. Data are presented as the mean values with error bars representing SD. Significance was determined using the Least Significant Difference method or Games-Howell test. *P<0.05, ***P<0.001. CVEC, canine vascular endothelial cells; LA20k9, Life Age 20k9; bFGF, basic fibroblast growth factor; SASP, senescence-associated secretory phenotype; DOX, doxorubicin; NC, negative control.

reactions and signal transduction. During cellular senescence, a decline in NAD^+ levels leads to mitochondrial dysfunction, reduced DNA repair capacity and increased inflammation. Supplementation with NAD^+ precursors, such as nicotinamide mononucleotide, has been shown to delay the aging process (33). Meanwhile, oxidative stress and inflammatory responses are recognized as the most significant exogenous factors triggering the senescence response (34).

In CVECs, after DOX treatment, the levels of inflammatory factors IL-1β, TNF-α, IL-6, IL-8, GM-CSF and MCP-1, as well as the oxidative stress-associated index MDA, significantly increased (P<0.05), while the NAD^+ content, SOD activity and GSH concentration significantly decreased (P<0.05; Figs. 4 and 5). After co-treatment with LA20k9, the levels of inflammatory factors and MDA decreased significantly (P<0.05), while the levels of NAD^+, SOD and GSH increased significantly (P<0.05). Specifically, IL-1β levels increased from 50.4 ng/ml (NC) to 174.5 ng/ml (DOX) and decreased to 86.8 ng/ml with DOX + LA20k9 treatment. TNF-α levels increased from 17.5 ng/ml (NC) to 38.3 ng/ml (DOX) and decreased to 22.9 ng/ml with DOX + LA20k9 treatment. IL-6 levels increased from 86.0 ng/ml (NC) to 116.2 ng/ml (DOX) and decreased to 92.9 ng/ml with DOX + LA20k9 treatment. IL-8 levels increased from 45.5 ng/ml (NC) to 55.1 ng/ml (DOX) and decreased to 45.6 ng/ml with DOX + LA20k9 treatment. GM-CSF levels increased from 174.0 ng/ml (NC) to 254.5 ng/ml (DOX) and decreased to 174.8 ng/ml with DOX + LA20k9 treatment. MCP-1 levels increased from 84.4 ng/ml (NC) to 95.7 ng/ml (DOX) and decreased to 83.6 ng/ml with DOX + LA20k9 treatment. MDA content increased from 0.151 μmol/mg prot (NC) to 0.162 μmol/mg prot (DOX) and decreased to 0.152 μmol/mg prot with DOX + LA20k9 treatment. NAD^+ content decreased from 0.978 μM (NC) to 0.426 μM (DOX) and increased to 0.719 μM with DOX + LA20k9 treatment. SOD activity decreased from 27.2 U/mg prot (NC) to 12.8 U/mg prot (DOX) and increased to 32.1 U/mg prot with DOX + LA20k9 treatment. GSH content decreased from 8.1 μM (NC) to 5.3 μM (DOX) and increased to 7.4 μM

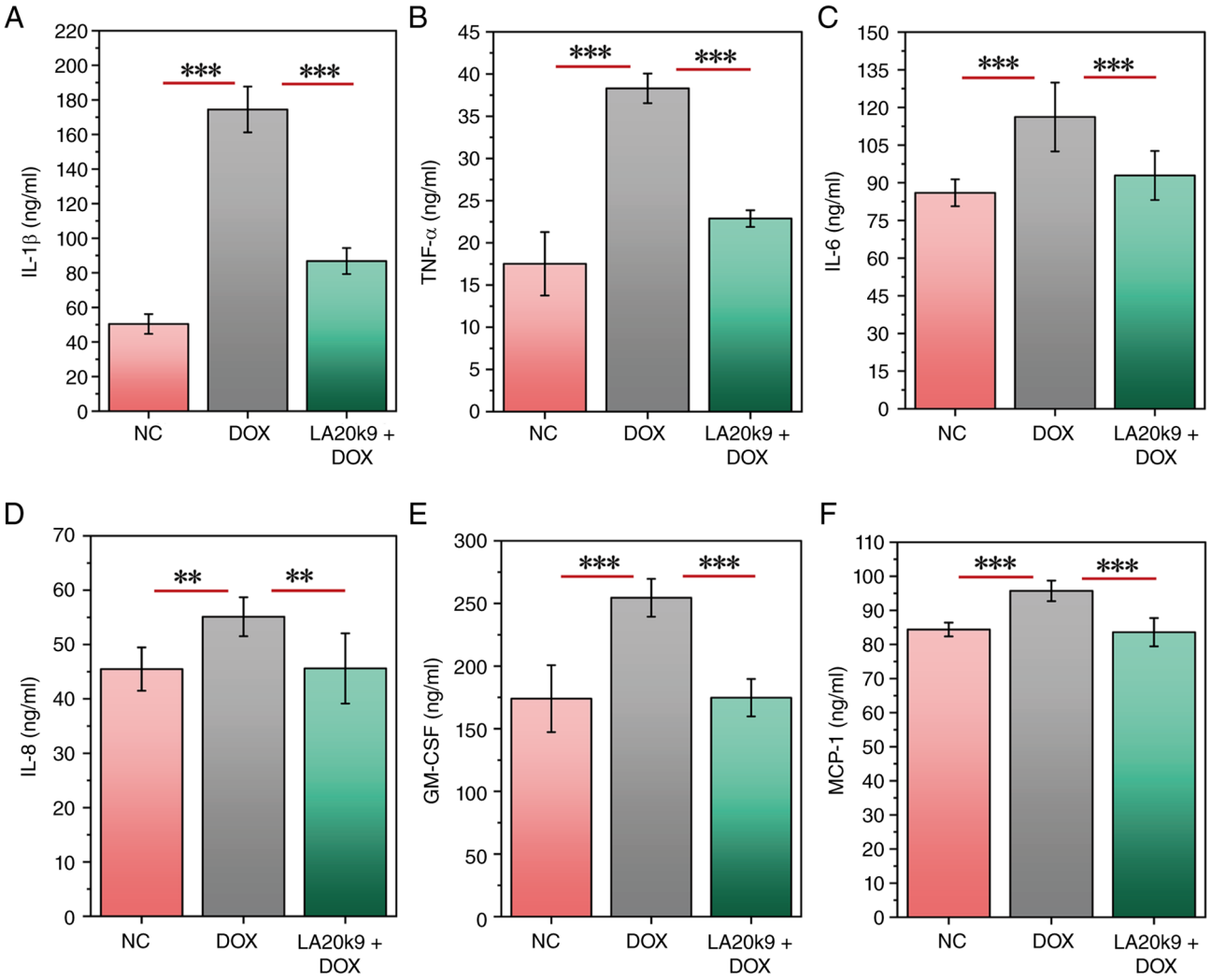

Figure 4. Effects of LA20k9 on inflammatory cytokine levels in CVECs. Levels of inflammatory cytokines, including (A) IL-1β, (B) IL-6, (C) IL-8, (D) TNF-α, (E) GM-CSF and (F) MCP-1 in CVECs. Inflammatory cytokine levels assays were performed with at least four replicates per group. Data are presented as the mean values with error bars representing SD. Significance was determined using the Least Significant Difference method or Games-Howell test. **P<0.01, ***P<0.001. CVEC, canine vascular endothelial cells; LA20k9, Life Age 20k9; DOX, doxorubicin; NC, negative control; MCP-1, chemoattractant protein-1; GM-CSF, granulocyte-macrophage colony-stimulating factor.

with DOX + LA20k9 treatment. These findings indicated that LA20k9 not only increased cell survival rates but also restored oxidative balance and reduced inflammatory responses.

Analysis of RNA-sequencing differential gene expression. Following transcriptome sequencing, 12 cDNA libraries were constructed, yielding a total of 35.68 Gb of raw data. The proportion of Q30 bases exceeded 95.25% across all samples, indicating high base-calling accuracy. Clean reads from each sample were aligned to the reference genome, with mapping efficiencies ranging from 85.03-92.94%. The results demonstrated that the sequencing quality for all samples was high and suitable for downstream analysis.

The mechanism of LA20k9 effect on aging was investigated by conducting a statistical analysis of the DEGs between the control group and the DOX-induced aging group, as well as between the DOX-induced aging group and the LA20k9 intervention group. Reliability was evaluated using Pearson's correlation coefficient (r). The results showed that the sample r^2 within each treatment group exceeded 0.80, indicating a strong correlation (Fig. 6A). Venn diagram analysis was used to present the number of DEGs, visually reflecting the overlapping associations among different DEG sets and the distribution of genes within each set. This provided clear and visual data support for subsequent research. Venn analysis showed that 454 genes were co-expressed in the NC group and the LA20k9 group (Fig. 6B). The expression profiles of the NC group and the LA20k9 group were more similar (Fig. 6C).

DEGs were screened based on changes in gene expression levels between the two sample groups and were further classified into upregulated and downregulated genes according to their expression trends. The statistical summary of DEGs between NC and DOX (Fig. 6D and E) showed that a total of 2,519 genes were upregulated including TOB1 (an anti-proliferative protein that negatively regulates cell cycle progression), UBR4, TM7SF2, TUBB4B, PIDD (a p53-induced death domain protein mediating apoptosis and cell cycle arrest), FOSL1, ESYT3, FAAH, CD70 and CHRD. Conversely, 3,888 genes were downregulated, including WDR75, CFI (a trypsin-like serine protease involved in complement system regulation),

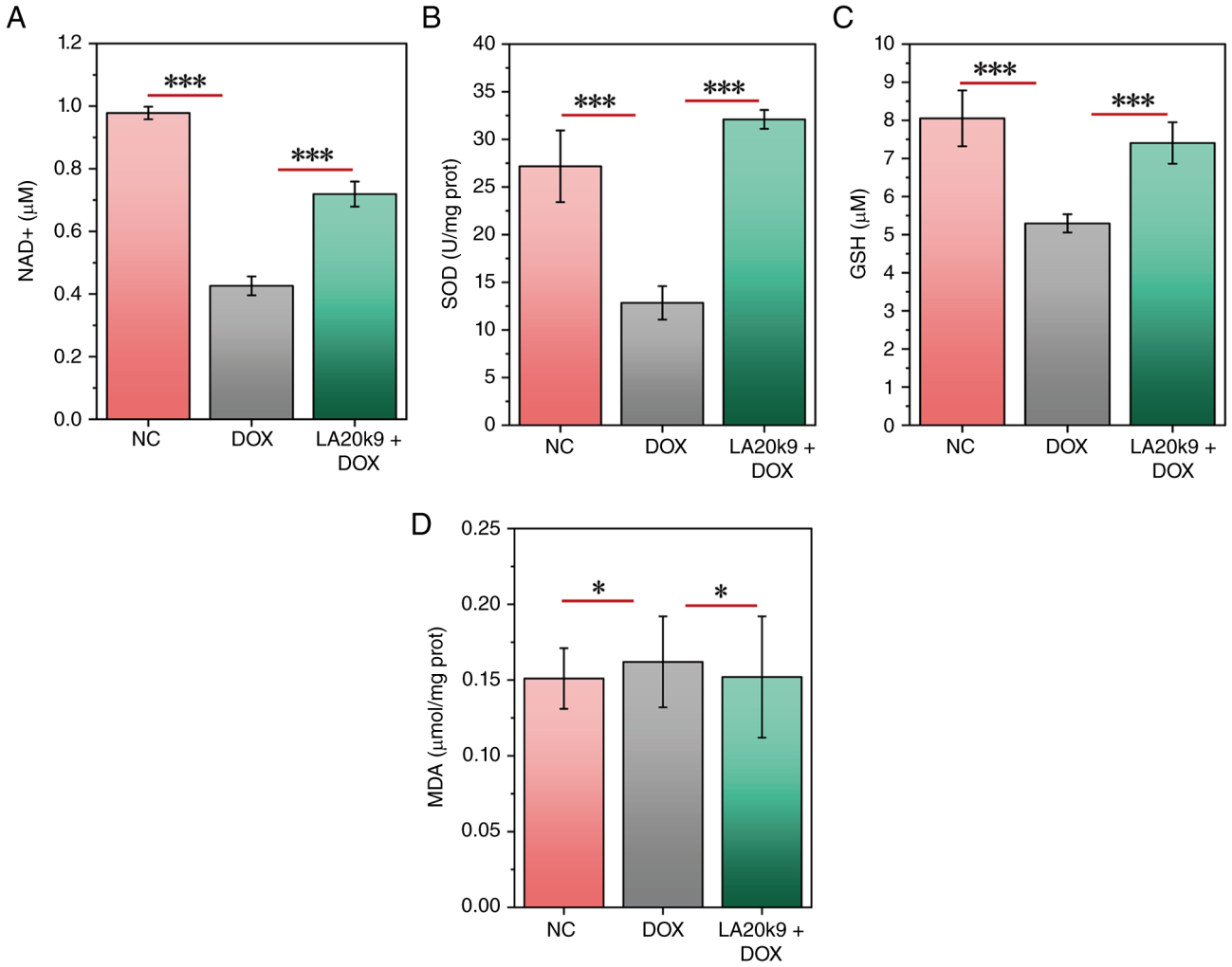

Figure 5. Effects of LA20k9 on NAD^+ and oxidative stress levels in CVECs. (A) Levels of NAD^+ in CVEC with DOX-induced senescence. CVEC were treated with 0.2 μmol/l DOX and 1,280 μg/ml LA20k9. Levels of oxidative stress markers, including (B) SOD, (C) GSH and (D) MDA in CVEC treated with 1,280 μg/ml LA20k9 and optimal DOX concentrations, showing significant improvements compared with the DOX-only group. NAD^+ and oxidative stress levels assays were performed with at least four replicates per group. Data are presented as the mean values with error bars representing SD. Significance was determined using the Least Significant Difference method or Games-Howell test. P-values indicate specific comparisons between the indicated groups. $^*P<0.05$, $^{***}P<0.001$. CVEC, canine vascular endothelial cells; LA20k9, Life Age 20k9; DOX, doxorubicin; NC, negative control; SOD, superoxide dismutase; MDA, malondialdehyde; GSH, glutathione.

HSPA13, MSH2, NOP58, CCDC112, SNX2, ZNF25, ETAA1 (an ATR kinase activator mediating replication stress response and genome stability maintenance) and NUDT12. The functional annotations of the DEGs between NC and DOX are described in Table SII.

The comparison of DOX and LA20k9 DEGs identified 4,120 upregulated genes, including EIF3E, CFI, SULT1C4, IMPACT, PPP4R2 (a regulatory subunit of protein phosphatase 4 mediating NF-κB signaling and DNA repair), SERINC1, SLC38A2, YME1L1, SCFD1 and ZC3H15 (a zinc-finger protein involved in mRNA processing and cellular homeostasis). By contrast, 2,915 genes were downregulated, including MKI67, INPP5J (an inositol 5-phosphatase regulating phosphoinositide signaling), PLA2G3 (a secretory phospholipase A2 associated with lipid metabolism and inflammation), CYR61 (a cellular communication network factor involved in cell adhesion, migration and stress responses), UBR4 (an E3 ligase associated with protein ubiquitination and stress signaling), TM7SF2, MVD, DHCR7, FADS2 and FASN. The functional annotations of the DEGs between DOX and LA20k9 are described in Table SIII. These results indicate that gene expression changed significantly under different treatment conditions and the data quality was reliable, making it suitable for subsequent in-depth analysis.

Analysis of differentially expressed genes: GO and KEGG analyses. GO and KEGG pathway enrichment analyses of DEGs in the NC vs. the DOX group and the DOX vs. the LA20k9 group were performed to explore the effect of LA20k9 treatment on the senescence response of CVECs.

The GO annotations of DEGs included three functional categories: Biological processes, cellular composition and molecular function (Fig. 6F and G). The top terms in the DOX group were 'chromosome', 'protein-DNA complex', 'nucleosome' and 'chromatin'. DOX exhibited an upregulatory effect on these biological functions. DOX induces DNA damage-dependent cellular senescence by intercalating into double-stranded DNA, triggering DNA damage and oxidative

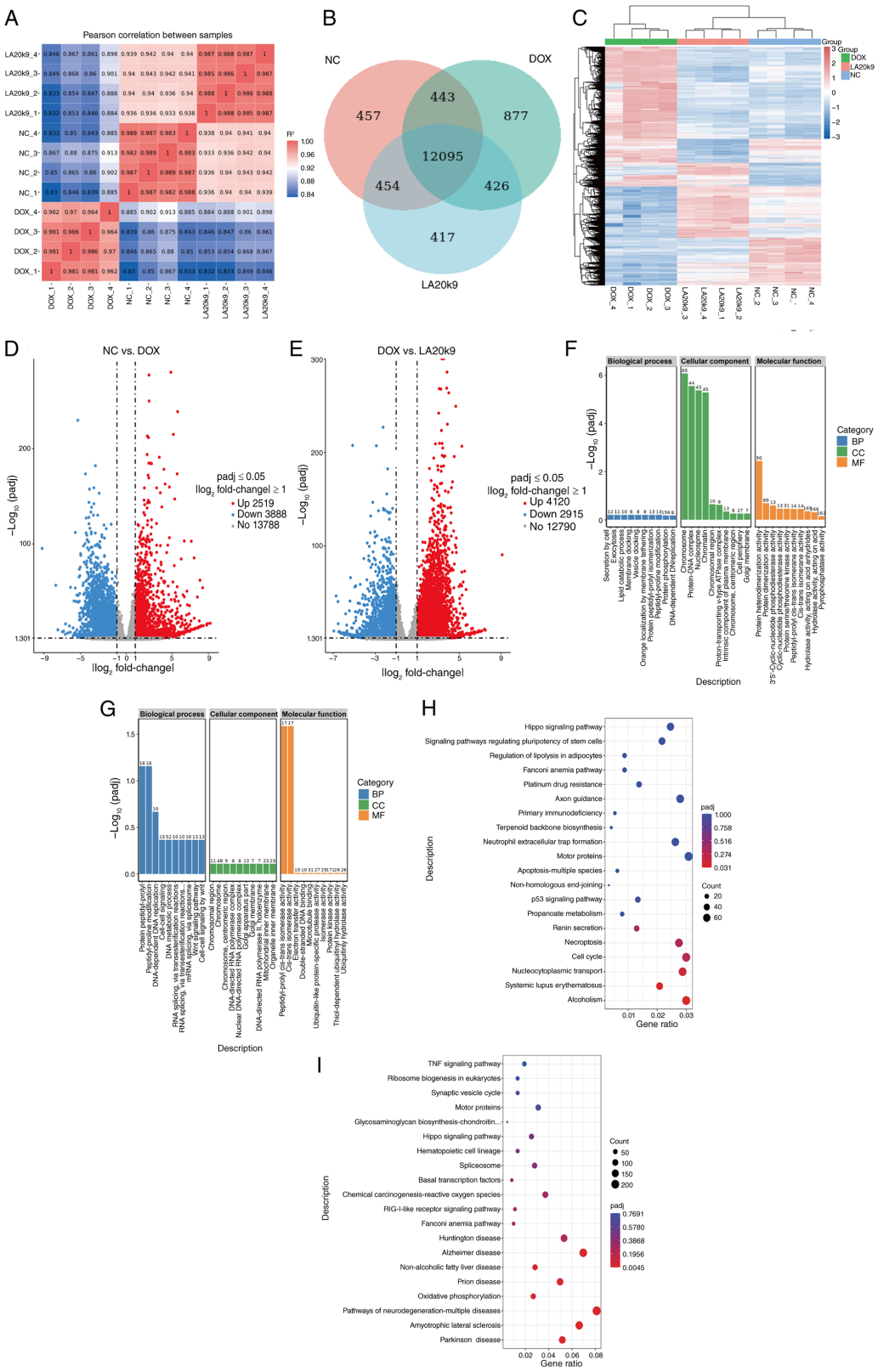

Figure 6. Transcriptomic analysis of in CVECs upon LA20k9 treatment. (A) Inter-sample correlation heat map, (B) Venn diagram and (C) and cluster heat map of CVECs treated with LA20k9. The volcano plot visually displays the distribution of differential genes in each comparison combination, including (D) DOX vs. NC and (E) LA20k9 vs. DOX. The abscissa in the figure represents the fold change of gene expression in the comparison group ($\log_2$ fold change) and the ordinate represents the significance level of the gene expression difference in the comparison group ($-\log_{10}$ P-value). Upregulated genes are represented by red dots and downregulated genes are represented by green dots. GO functional enrichment histogram for DOX (F) and LA20k9 (G). The ordinate is the significance level of GO term enrichment. The value on the column represents the number of differential genes enriched for this term. Different colors represent the three GO subcategories of biological processes, cellular components and molecular functions, respectively. KEGG pathway enrichment bubble plot of DOX (H) and LA20k9 (I). The abscissa in the figure is the ratio of the number of differential genes annotated to the KEGG pathway to the total number of differential genes. The ordinate is the KEGG pathway. The size of the dot represents the number of genes annotated to the KEGG pathway. Transcriptome sequencing was performed with at least four replicates per group. CVEC, canine vascular endothelial cell; LA20k9, Life Age 20k9; DOX, doxorubicin; NC, negative control; padj, adjusted P-value; UP, upregulated; DOWN, downregulated; GO, Gene Ontology; KEGG, Kyoto Encyclopedia of Genes and Genomes.

stress (35,36). During this process, transcriptomic analysis revealed significant associations with cellular composition elements, including chromosomes, chromatin, nucleosomes and DNA-protein complexes. These changes are closely associated with chromatin remodeling and structural reinforcement that occur in senescent cells to maintain genomic stability. The most abundant terms in the LA20k9 group were 'peptidyl-prolyl cis-trans isomerase activity', 'cis-trans isomerase activity', 'protein peptidyl-prolyl isomerization' and 'peptidyl-proline modification'. Transcriptome analysis demonstrated that LA20k9 exhibited a downregulatory effect on these biological functions. This suggested that LA20k9 may exert the function associated with peptidyl-prolyl cis-trans isomerase, reduce the levels of protein peptidyl-prolyl isomerization and modification, thereby inhabiting the excessive activation of the p53-centered senescence pathway, which may prevent the sustained amplification of DNA damage downstream signaling. Ultimately, this effects may help alleviate cellular senescence and restore the normal cellular state. Therefore, the downregulation of these functions is highly consistent with the anti-senescence effect of LA20k9 against DOX-induced senescence, suggesting that inhibiting peptidyl-prolyl cis-trans isomerase-associated activities may represent an important molecular mechanism underlying the protective effect of LA20k9.

Further KEGG pathway enrichment analysis was performed to systematically characterize the functional distribution of DEGs at the signaling pathway level. The top 20 most significantly enriched pathways are displayed in Fig. 6H and I. DOX treatment was associated with the enrichment of genes involved in the 'p53 signaling pathway', a core regulatory cascade governing the DNA damage response, cell cycle arrest, apoptosis and cellular senescence. Mechanistically, DOX upregulated a series of pivotal genes in this pathway, including ATR, SESN2, GADD45G, PIDD, CCNG1/2, TP73, ZNF385A and GADD45B. Meanwhile, DOX downregulated CCNE1 and CCNE2. Collectively, these transcriptomic changes suggest that DOX may trigger the robust activation of the p53-dependent DNA damage surveillance network, which, in turn, promotes growth arrest, DNA repair responses, apoptosis and stress-associated signaling, ultimately leading to permanent cell cycle exit and establishing cellular senescence in CVECs.

Further mechanistic insight was obtained by examining the regulatory effects of LA20k9 on key signaling and functional pathways. LA20k9 was associated with the enrichment of genes involved in homologous recombination and cell cycle regulation, while concurrently suppressing pathways associated with chemical carcinogenesis and reactive oxygen species (ROS)-driven genotoxicity. At the molecular level, these protective effects were associated with the upregulation of a core set of genes key in DNA double-strand break repair, DNA replication and cell cycle progression, including RPA1, UIMC1, BRIP1, MRE11A, POLD3, MCM2, MCM3, RAD21, ORC4, ORC5 and CCNE2. In addition, LA20k9 enhanced the expression of genes involved in anti-inflammatory and cytoprotective signaling, such as TANK, ATG5 and CHUK. Concomitantly, LA20k9 downregulated genes associated with mitochondrial dysfunction, oxidative stress and ROS-mediated cellular damage, including UQCRC1, CYP1A1 and SLC25A5. Collectively, these findings indicate that LA20k9 exerts its senescence-attenuating effects by restoring homologous recombination-mediated DNA repair, sustaining normal cell cycle progression and alleviating ROS-associated oxidative injury. The present findings suggest that LA20k9 could effectively counteract the deleterious senescence program triggered by DOX, possibly through reinforcing genomic stability, reducing oxidative stress and normalizing cell cycle dynamics, thus potentially protecting cells against DNA damage-induced growth arrest and functional decline.

Analysis of non-targeted metabolome results. LA20k9 anti-aging mechanism was analyzed using non-targeted metabolomics technology. Based on the aforementioned data, systematic pathway annotations were made for all identified metabolites and differential analysis and KEGG analysis were conducted for all differentially expressed metabolites. Metabolites were classified according to their chemical structure, among which, lipids and lipid-like molecules (29.22%) accounted for a relatively high proportion (Fig. 7A). Venn diagrams visually present the overlap and unique metabolites between different groups, and illustrate the relationships between multiple groups of differentially expressed metabolites (Fig. 7B). Hierarchical cluster analysis showed that the metabolic patterns of the NC and LA20k9 groups were similar (Fig. 7C).

Relative to the NC group, the levels of terezine A, parinol, metomidate, methylaphyllate, pyro-L-glutaminyl-L-glutamine, 9(11)-dehydroaxinystero, pentylone and arginyltryptophan were significantly upregulated in the DOX group (Tables I and II). The majority of these metabolites are closely associated with oxidative stress, inflammatory activation and endothelial dysfunction, which are key pathogenic characteristics of vascular ECs senescence. By contrast, monolaurin, (6E,10E)-2,6,10-trimethyldodeca-2,6,10-triene, clitocybulol B, 3-oxotetradecanoic acid, prosopinine and (E,E)-12-hydroxy-6,10-dimethyl-6,10-dodecadien-2-one were significantly upregulated in the LA20k9 group compared with the DOX group. These metabolites are primarily involved in anti-inflammatory responses, maintaining membrane stability, improving lipid metabolism and enhancing endothelial protection, thereby contributing to the alleviation of vascular endothelial senescence (37-40).

KEGG pathway analysis indicated that 'global and overview maps' and 'lipid metabolism' contained the highest number of differentially expressed metabolites in both the DOX and LA20k9 groups, suggesting that metabolic reprogramming and lipid homeostasis are key in regulating vascular ECs senescence (Fig. 7D and E). Enrichment analysis revealed that pathways including 'caffeine metabolism', 'thyroid hormone synthesis', 'ether lipid metabolism' and 'asthma' were significantly enriched in the DOX group compared with the NC group, with the largest number of differential metabolites involved in 'glycerophospholipid metabolism', 'choline metabolism in cancer', 'efferocytosis' and 'steroid hormone biosynthesis' (Fig. 7F and G). These pathways are closely associated with oxidative stress injury, mitochondrial dysfunction, inflammatory responses and endothelial barrier damage, all of which promote the occurrence and progression of vascular endothelial senescence

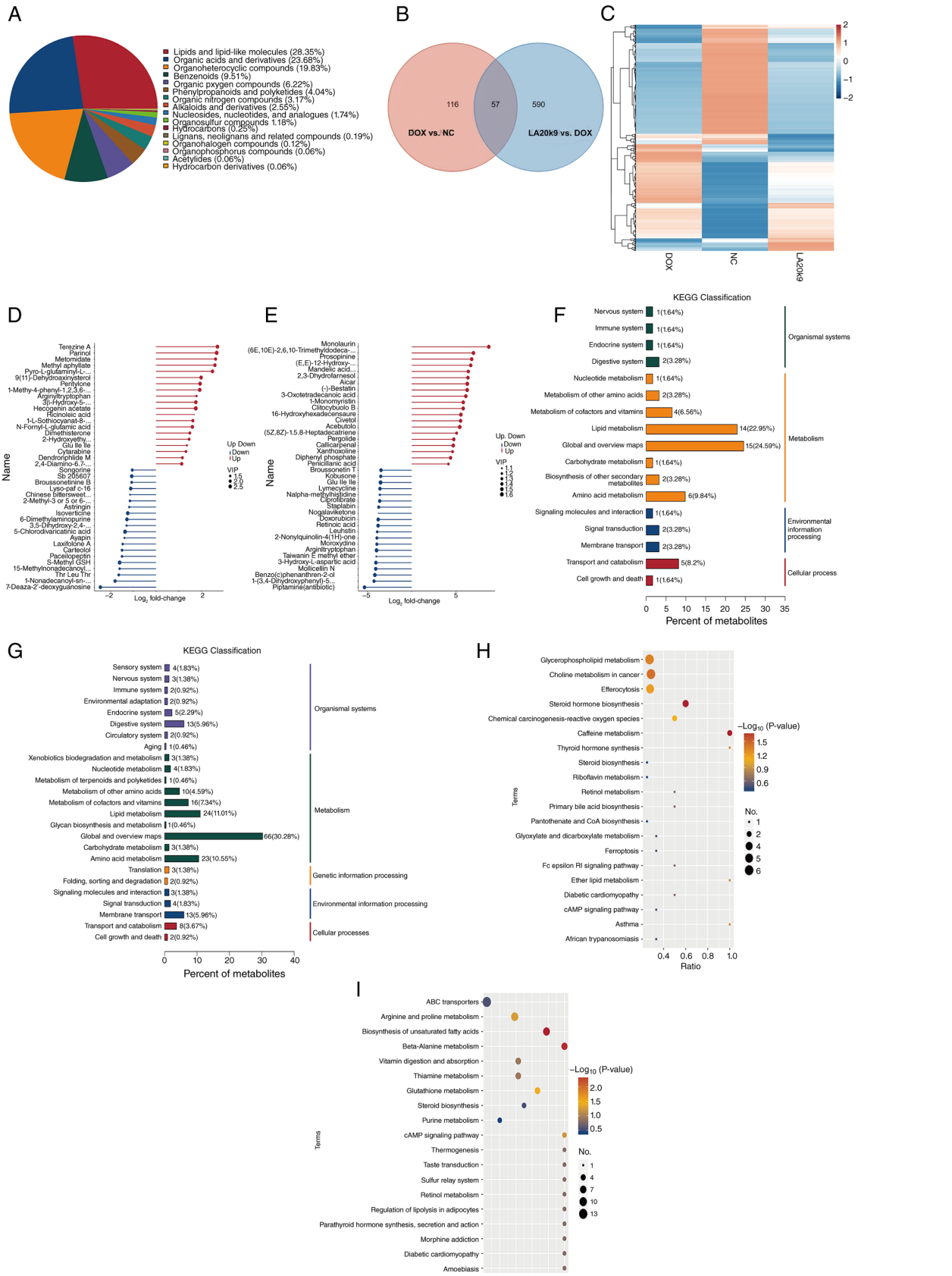

Figure 7. Metabolomics analysis of in CVECs upon LA20k9 treatment. (A) Piece chart, (B) Venn diagram and (C) cluster heat map of the proportion of metabolites in CVECs treated with LA20k9. KEGG pathway annotation diagrams of (D) DOX and (E) LA20k9. KEGG pathway enrichment bubble diagrams of (F) DOX and (G) LA20k9. KEGG pathway enrichment bubble diagrams of (H) DOX and (I) LA20k9. Red represents up-regulated metabolites and blue represents down-regulated metabolites. The horizontal axis in the figure is x/y (the number of differential metabolites in the corresponding metabolic pathway/the total number of metabolites identified in the pathway). The color of the point represents the P-value. Non-targeted metabolomics were performed with at least four replicates per group. CVEC, canine vascular endothelial cells; LA20k9, Life Age 20k9; DOX, doxorubicin; NC, negative control; KEGG, Kyoto Encyclopedia of Genes and Genomes.

Table I. Differential metabolites of doxorubicin vs. negative control.

Metabolite name	FC	$\log_2$ FC	Up or down	P-value	VIP
1-methyl-4-phenyl-1,2,3,6-2-tetrahydropyridine N-oxide	3.781	1.919	Up	0.006	2.551
Metomidate	6.127	2.615	Up	0.044	1.928
Pentylone	3.822	1.934	Up	0.004	2.576
Pyro-L-glutaminyl-L-glutamine	5.567	2.477	Up	0.011	2.304
Terezine A	6.485	2.697	Up	0.001	2.537
Methyl aphyllate	5.998	2.585	Up	0.024	2.343
Parinol	6.321	2.660	Up	0.004	2.759
9(11)-dehydroaxinysterol	3.942	1.979	Up	0.010	2.490
Arginyltryptophan	3.422	1.775	Up	0.034	1.414
3-β-hydroxy-5-cholestenoic acid	3.354	1.746	Up	0.021	2.419
Ayapin	0.383	-1.385	Down	<0.001	1.224
Paecilopeptin	0.355	-1.492	Down	0.010	1.503
7-deaza-2'-deoxyguanosine	0.184	-2.440	Down	<0.001	2.305
Carteolol	0.356	-1.491	Down	0.011	1.646
S-methylglutathione	0.331	-1.596	Down	0.002	2.664
Threonine-leucine-threonine	0.322	-1.634	Down	0.005	1.659
Laxifolone A	0.363	-1.461	Down	0.029	1.491
methylnonadecanoyl-carnitine	0.331	-1.597	Down	0.019	1.449
1-nonadecanoyl-sn-glycero-3-phosphocholine	0.288	-1.796	Down	0.025	2.151
5-chlorodivaricatinic acid	0.390	-1.358	Down	0.001	2.700

Differential metabolite screening mainly refers to three parameters: VIP, FC and P-value. VIP refers to the first principal component of the PLS-DA model and the VIP value indicated the contribution of metabolites to the grouping. FC refers to the ratio of the mean values of all biological replicate quantification values of each metabolite in the comparison group. P-values were calculated through a t-test and represented the level of significance of the difference. The thresholds were set as VIP >1.0, FC >1.2 or FC <0.833 and P<0.05 to screen out the differential metabolites. VIP, variable importance in the projection; FC, fold change; Down, downregulation; Up, upregulation.

induced by DOX (41-44). Conversely, compared with the DOX group, the LA20k9 group showed significant enrichment in the 'cAMP signaling pathway', 'amino sugar and nucleotide sugar metabolism', 'parathyroid hormone synthesis, secretion and action' and 'retinol metabolism' pathways. The most highly represented pathways included 'ABC transporters', 'arginine and proline metabolism', 'biosynthesis of unsaturated fatty acids', 'β-alanine metabolism' and 'vitamin digestion and absorption'. The cAMP pathway protects endothelial function by mitigating inflammation, oxidative stress and SASP. Retinol metabolism sustains endothelial integrity and delays senescence. Arginine/proline metabolism optimizes vascular homeostasis, while unsaturated fatty acid biosynthesis preserves membrane and mitochondrial function. ABC transporters alleviate intracellular metabolic damage (45-49). This result therefore suggests that LA20k9 improves vascular endothelial function and resists cellular senescence mainly by regulating metabolic homeostasis, activating the cAMP signaling pathway to inhibit inflammation and oxidative stress, enhancing retinol metabolism and endothelial repair capacity and maintaining lipid balance and mitochondrial function, thereby exerting protective effects against DOX-induced vascular ECs senescence.

Discussion

CVDs represent a leading cause of morbidity and mortality in the elderly population and advancing age is recognized as a key risk factor for the development and progression of CVDs (2). Although previous studies have demonstrated that fermented plant-derived extracts exhibit promising cardiovascular protective potential due to their antioxidant, anti-inflammatory, antimicrobial and organ-protective properties (50-52), such investigations have generally been limited by the use of non-species-specific probiotic strains, cross-species cellular models and insufficient mechanistic validation.

The present study advances this field through three dimensions. First, a novel canine-specific probiotic strain (*Bifidobacterium adolescentis* Life Age 20-k9) isolated from long-lived dogs was employed, which better matches canine physiological and pathological features and thereby improves biological relevance. Second, mechanistic investigations were performed in a targeted CVECs model rather than relying on cross-species systems, thus minimizing interspecies variation and enabling species-specific insights into vascular endothelial senescence. Third, by integrating functional assays, transcriptomics and metabolomics, deeper multi-omics mechanistic evidence that extends beyond preliminary efficacy

Table II. Differential metabolites of Life Age 20k9 vs. doxorubicin.

Metabolite name	FC	log_2 FC	P-value	Up or down	VIP
1-monomyristin	56.856	5.829	0.001	Up	1.467
Monolaurin	418.773	8.710	0.001	Up	1.533
3-oxotetradecanoic acid	69.435	6.118	0.001	Up	1.477
(6E,10E)-2,6,10-trimethyldodeca-2,6,10-triene	126.006	6.977	0.001	Up	1.508
(E,E)-12-hydroxy-6,10-dimethyl-6,10-dodecadien-2-one	101.728	6.669	0.001	Up	1.455
2,3-dihydrofarnesol	81.933	6.356	0.001	Up	1.454
Prosopinine	109.734	6.778	0.001	Up	1.483
5-aminoimidazole-4-carboxamide ribonucleoside	77.808	6.282	0.001	Up	1.564
(-)-Bestatin	77.182	6.270	0.001	Up	1.527
Mandelic acid, methyl ester	84.517	6.401	0.001	Up	1.386
Piptamine (antibiotic)	0.025	-5.337	0.001	Down	1.473
Mollicellin N	0.060	-4.068	0.001	Down	1.464
Benzo (c)phenanthren-2-ol	0.056	-4.166	0.001	Down	1.550
Taiwanin E methyl ether	0.062	-4.011	0.002	Down	1.095
3-hydroxy-L-aspartic acid	0.060	-4.050	0.002	Down	1.488
1-(3,4-dihydroxyphenyl)-5-hydroxy-3-decanone	0.052	-4.259	0.002	Down	1.389
Arginyltryptophan	0.064	-3.974	0.002	Down	1.562
2-nonylquinolin-4(1H)-one	0.065	-3.935	0.002	Down	1.321
Leuhistin	0.067	-3.900	0.002	Down	1.242
Moroxydine	0.065	-3.940	0.002	Down	1.340

Differential metabolite screening mainly refers to three parameters: VIP, FC, and P-value. VIP refers to the first principal component of the PLS-DA model and the VIP value indicated the contribution of metabolites to the grouping. FC refers to the ratio of the mean values of all biological replicate quantification values of each metabolite in the comparison group. P-value was calculated through a t-test and represented the level of significance of the difference. The thresholds were set as VIP >1.0, FC >1.2 or FC <0.833 and P<0.05 to screen out the differential metabolites. VIP, variable importance in the projection; FC, fold change; Down, downregulation; Up, upregulation.

observations and reveals key regulatory pathways underlying the anti-senescent effects was provided, including the p53 signaling pathway, cell cycle progression, cAMP signaling and retinol metabolism.

In the present study, LA20k9 enhanced cell viability and reduced the release of SA-β-gal activity associated with aging. Only an LA20k9 concentration of 1,280 μg/ml enhanced the NAD^+ content in CVECs. In normal cells, the SASP gene is typically tightly suppressed to prevent the inappropriate expression of inflammatory signals. However, in senescent cells, the SASP gene becomes highly upregulated (53). Elevated MMP expression has been shown to promote the degradation of extracellular matrix components, such as collagen fibers and hyaluronic acid, thereby accelerating cellular aging (54,55). With respect to endothelial function, VEGF exerts pleiotropic effects on vascular ECs, promoting angiogenesis by stimulating ECs proliferation and migration, as well as modulating gene expression profiles. Notably, VEGF has been reported to delay the onset of senescence in microvascular ECs and potentially reverse age-associated changes (56). Furthermore, certain FGF family members, including bFGF, serve key roles in metabolic regulation and tissue homeostasis, supporting the regeneration of damaged tissues and facilitating the repair of aged tissues (57). Treatment with LA20k9 decreased MMP-1 and MMP-3 content and increased VEGF and bFGF content in DOX-stimulated aging CVECs. Aging cells produce a number of inflammatory cytokines and an increase in inflammatory factors will accelerate cellular senescence (58). Treatment with LA20k9 decreased IL-1β, IL-6, IL-8, MCP-1, GM-CSF and TNF-α content in DOX-stimulated aging CVECs. LA20k9 also alleviated the oxidative damage caused by DOX induction.

The functions of key signaling pathways and their regulation by LA20k9 were systematically summarized to further understand the anti-aging mechanisms of LA20k9. The p53 signaling pathway is a central pathway governing cell survival, DNA damage repair, cell cycle progression and apoptosis. As a key tumor suppressor, p53 is activated under stress conditions such as DNA damage and then stabilized through phosphorylation and acetylation (59,60). Activated p53 upregulates p21WAF1/CIP1 and 14-3-3σ, leading to cell cycle arrest in the G_1/S and G_2/M phases. In the present study, DOX significantly increased the mRNA expression of ATR, SESN2, GADD45G, PIDD and TP73, suggesting that the p53 pathway may be activated, which may have promoted DNA damage, apoptosis and cellular senescence in CVECs (61). LA20k9 could counteract these effects by potentially upregulating homologous recombination and normal cell cycle progression, while possibly downregulating chemical carcinogenesis-ROS, which may contribute to the alleviation of DOX-induced senescence.

The cAMP signaling pathway functions as a central second-messenger system involved in mitochondrial function, oxidative stress and aging. cAMP is synthesized from ATP by adenylate cyclase and acts through downstream effectors, including cyclic-AMP dependent protein kinase A, exchange protein activated by cAMP and cyclic nucleotide gated ion channels. This pathway is widely implicated in age-associated cardiovascular and metabolic diseases (62-67). In the present study, non-targeted metabolomics suggested that LA20k9 may activate the cAMP signaling pathway, which could contribute to improved mitochondrial function as well as potentially reduced cellular senescence and inflammation. Retinol metabolism is another key pathway regulating extracellular matrix synthesis and anti-aging processes. Retinol promotes the production of collagen and glycosaminoglycans, inhibits MMP activity and exerts antioxidant effects (68,69). The present study suggested that LA20k9 may activate retinol metabolism, potentially accelerate collagen formation and appear to suppress matrix degradation, thereby possibly delaying cellular senescence at the metabolic level. Collectively, LA20k9 may attenuate endothelial senescence by coordinately regulating the p53 signaling pathway, cAMP signaling pathway and retinol metabolism, which may exert distinct but complementary functions.

In conclusion, the evidence reported in the present study demonstrated that LA20k9 exerted a significant anti-aging protective effect in CVECs. LA20k9 markedly enhanced cell viability and reduced senescence-associated SA-β-Gal activity. Furthermore, LA20k9 significantly downregulated the expression of aging-associated phenotypic markers MMP-1 and MMP-3, while concomitantly increasing VEGF and bFGF levels, which were important for vascular integrity and function. Notably, LA20k9 mitigated DOX-induced stress injury by increasing intracellular levels of NAD^+, SOD and GSH and reducing MDA concentrations.

At the transcriptional level, LA20k9 counteracted DOX-induced cellular senescence by promoting normal cell-cycle progression and suppressing chemical carcinogenesis-ROS. At the metabolic level, it activated the cAMP signaling pathway and retinol metabolism, thereby restoring mitochondrial function and suppressing cellular senescence and inflammatory responses. These results underscore the therapeutic potential of LA20k9 in combating vascular aging and improving vascular health. The findings of the present study support the development of post-biological agents as a novel and promising strategy for ameliorating age-related cardiovascular decline in animals.

Despite this, the present study has its limitations, mainly reflected in the following two aspects: First, the present study was conducted only at the *in vitro* cellular level to investigate anti-aging effects, lacking corresponding *in vivo* validation using animal models; and second, the underlying anti-aging mechanisms remain to be further elucidated, especially through verification in appropriate animal models. In the future, animal experiments will be carried out *in vivo* by establishing a mouse model to systematically explore the anti-aging effects of metabolites derived from brown algae extract fermented by canine-origin *Bifidobacterium*. Despite these limitations, the present study still provides valuable insights into the development of postbiotic fermented metabolites with anti-aging properties and their potential applications in anti-aging research.

Acknowledgements

Not applicable.

Funding

No funding was received.

Availability of data and materials

The RNA-sequencing data generated in the present study may be found in the NCBI Sequence Read Archive under accession number PRJNA1451389 or at the following URL: https://www.ncbi.nlm.nih.gov/search/all/?term=PRJNA1451389. The metabolomics data generated in the present study may be found in the Open Archive for Miscellaneous Data (China National Center for Bioinformation/Beijing Institute of Genomics, Chinese Academy of Sciences) under accession number OMIX016205 or at the following URL: https://ngdc.cncb.ac.cn/omix/release/OMIX016205.

Authors' contributions

HCJ designed the present research and wrote the original manuscript draft. HSB, TL and HYW analyzed the experimental data. YLL and ZZW participated in the conception and design of the research, provided resources and supervised the work. HCJ, HSB, TL, HYW, YLL and ZZW confirm the authenticity of all the raw data. All authors read and approved the final version of the manuscript.

Ethics approval and consent to participate

Not applicable.

Patient consent for publication

Not applicable.

Competing interests

The authors declare that they have no competing interests.

References

1. López-Otín C, Blasco MA, Partridge L, Serrano M and Kroemer G: Hallmarks of aging: An expanding universe. Cell 186: 243-278, 2023.
2. Chmielewski PP, Data K, Strzelec B, Farzaneh M, Anbiyaiee A, Zaheer U, Uddin S, Sheykhi-Sabzehpoush M, Mozdziak P, Zabel M, *et al*: Human aging and age-related diseases: From underlying mechanisms to pro-longevity interventions. Aging Dis 16: 1853-1877, 2024.
3. Augustin HG and Koh GY: A systems view of the vascular endothelium in health and disease. Cell 187: 4833-4858, 2024.
4. Fajemiroye JO, da Cunha LC, Saavedra-Rodríguez R, Rodrigues KL, Naves LM, Mourão AA, da Silva EF, Williams NEE, Martins JLR, Sousa RB, *et al*: Aging-induced biological changes and cardiovascular diseases. Biomed Res Int 2018: 7156435, 2018.

5. Li Z, Zhang Z, Ren Y, Wang Y, Fang J, Yue H, Ma S and Guan F: Aging and age-related diseases: From mechanisms to therapeutic strategies. Biogerontology 22: 165-187, 2021.
6. Xie S, Xu SC, Deng W and Tang Q: Metabolic landscape in cardiac aging: Insights into molecular biology and therapeutic implications. Signal Transduct Target Ther 8: 114, 2023.
7. Gude NA, Broughton KM, Firouzi F and Sussman MA: Cardiac ageing: Extrinsic and intrinsic factors in cellular renewal and senescence. Nat Rev Cardiol 15: 523-542, 2018.
8. Pagan LU, Gomes MJ, Gatto M, Mota GAF, Okoshi K and Okoshi MP: The role of oxidative stress in the aging heart. Antioxidants (Basel) 11: 336, 2022.
9. Zhang L, Pitcher LE, Yousefzadeh MJ, Niedernhofer LJ, Robbins PD and Zhu Y: Cellular senescence: A key therapeutic target in aging and diseases. J Clin Invest 132: e158450, 2022.
10. Campisi J, Andersen JK, Kapahi P and Melov S: Cellular senescence: A link between cancer and age-related degenerative disease? Semin Cancer Biol 21: 354-359, 2011.
11. Minamino T, Miyauchi H, Yoshida T, Ishida Y, Yoshida H and Komuro I: Endothelial cell senescence in human atherosclerosis: Role of telomere in endothelial dysfunction. Circulation 105: 1541-1544, 2002.
12. Bu LL, Yuan HH, Xie LL, Guo MH, Liao DF and Zheng XL: New dawn for atherosclerosis: Vascular endothelial cell senescence and death. Int J Mol Sci 24: 15160, 2023.
13. Lewis-McDougall FC, Ruchaya PJ, Domenjo-Vila E, Shin Teoh T, Prata L, Cottle BJ, Clark JE, Punjabi PP, Awad W, Torella D, *et al*: Aged-senescent cells contribute to impaired heart regeneration. Aging cell 18: e12931, 2019.
14. Yu S, Kim SR, Jiang K, Ogrodnik M, Zhu XY, Ferguson CM, Tchkonia T, Lerman A, Kirkland JL and Lerman LO: Quercetin Reverses cardiac systolic dysfunction in mice fed with a high-fat diet: Role of angiogenesis. Oxid Med Cell Longev 2021: 8875729, 2021.
15. Wang L, Wang B, Gasek NS, Zhou Y, Cohn RL, Martin DE, Zuo W, Flynn WF, Guo C, Jellison ER, *et al*: Targeting $p21^{Cipl}$ highly expressing cells in adipose tissue alleviates insulin resistance in obesity. Cell Metab 34: 75-89.e8, 2022.
16. Bloom SI, Islam MT, Lesniewski LA and Donato AJ: Mechanisms and consequences of endothelial cell senescence. Nat Rev Cardiol 20: 38-51, 2023.
17. Thorakkattu P, Khanashyam AC, Shah K, Babu KS, Mundanat AS, Deliephan A, Deokar GS, Santivarangkna C and Nirmal NP: Postbiotics: Current trends in food and pharmaceutical industry. Foods 11: 3094, 2022.
18. Wegh CAM, Geerlings SY, Knol J, Roeselers G and Belzer C: Postbiotics and their potential applications in early life nutrition and beyond. Int J Mol Sci 20: 4673, 2019.
19. Leser T and Baker A: *Bifidobacterium adolescentis*-a beneficial microbe. Benef Microbes 14: 525-551, 2023.
20. Li Y, Wang Y, Lu Y, Zhang M, Yan Z, Daun Y and Ma H: Breeding and application effect evaluation of *Bifidobacterium adolescentis* derived from felines with long life spans. Acta Microbiol Sin 65: 4938-4950, 2025.
21. Zhu M, Hsu CW, Peralta Ogorek LL, Taylor IW, La Cavera S, Oliveira DM, Verma L, Mehra P, Mijar M, Sadanandom A, *et al*: Single-cell transcriptomics reveal how root tissues adapt to soil stress. Nature 642: 721-729, 2025.
22. Schrimpe-Rutledge AC, Codreanu SG, Sherrod SD and McLean JA: Untargeted metabolomics strategies-challenges and emerging directions. J Am Soc Mass Spectrom 27: 1897-1905, 2016.
23. Mohammed Y, Pan J, Zhang S, Han J and Borchers CH: ExSTA: External standard addition method for accurate high-throughput quantitation in targeted proteomics experiments. Proteomics Clin Appl 12: 1600180, 2018.
24. Moskovets E, Chen HS, Pashkova A, Rejtar T, Andreev V and Karger BL: Closely spaced external standard: A universal method of achieving 5 ppm mass accuracy over the entire MALDI plate in axial matrix-assisted laser desorption/ionization time-of-flight mass spectrometry. Rapid Commun Mass Spectrom 17: 2177-2187, 2003.
25. Wu JL, Wu QP, Yang XF, Wei MK, Zhang JM, Huang Q and Zhou XY: L-malate reverses oxidative stress and antioxidative defenses in liver and heart of aged rats. Physiol Res 57: 261-268, 2008.
26. Fang W, Chen S, Jin X, Liu S, Cao X and Liu B: Metabolomics in aging research: Aging markers from organs. Front Cell Dev Biol 11: 1198794, 2023.
27. Chen X, Wu R, Li L, Zeng Y, Chen J, Wei M, Feng Y, Chen G, Wang Y, Lin L, *et al*: Pregnancy-induced changes to the gut microbiota drive macrophage pyroptosis and exacerbate septic inflammation. Immunity 56: 336-352.e9, 2023.
28. Zeng Y, Wu R, Wang F, Li S, Li L, Li Y, Qin P, Wei M, Yang J, Wu J, *et al*: Liberation of daidzein by gut microbial β-galactosidase suppresses acetaminophen-induced hepatotoxicity in mice. Cell Host Microbe 31: 766-780.e7, 2023.
29. D'Ambrosio M and Gil J: Reshaping of the tumor microenvironment by cellular senescence: An opportunity for senotherapies. Dev Cell 58: 1007-1021, 2023.
30. Hou J and Kim S: Possible role of ginsenoside Rb1 in skin wound healing via regulating senescent skin dermal fibroblast. Biochem Biophys Res Commun 499: 381-388, 2018.
31. Huang YH, Chen MH, Guo QL, Chen ZX, Chen QD and Wang XZ: Interleukin-10 induces senescence of activated hepatic stellate cells via STAT3-p53 pathway to attenuate liver fibrosis. Cell Signal 66: 109445, 2020.
32. Mosteiro L, Pantoja C, Alcazar N, Marión RM, Chondronasiou D, Rovira M, Fernandez-Marcos PJ, Muñoz-Martin M, Blanco-Aparicio C, Pastor J, *et al*: Tissue damage and senescence provide critical signals for cellular reprogramming in vivo. Science 354: aaf4445, 2016.
33. Ungvari Z, Tarantini S, Kiss T, Wren JD, Giles CB, Griffin CT, Murfee WL, Pacher P and Csiszar A: Endothelial dysfunction and angiogenesis impairment in the ageing vasculature. Nat Rev Cardiol 15: 555-565, 2018.
34. Huang W, Hickson LJ, Eirin A, Kirkland JL and Lerman LO: Cellular senescence: The good, the bad and the unknown. Nat Rev Nephrol 18: 611-627, 2022.
35. Huang P, Bai L, Liu L, Fu J, Wu K, Liu H, Liu Y, Qi B and Qi B: Redd1 knockdown prevents doxorubicin-induced cardiac senescence. Aging (Albany NY) 13: 13788-13806, 2021.
36. Shiheido-Watanabe Y, Sung EA, Ivessa A, Zhai P, Takada T, Ikeda S, Matsushita M, Zablocki D and Sadoshima J: Inhibition of PAI-1 shifts cardiomyocyte fate from senescence toward apoptosis and mitigates doxorubicin-induced cardiotoxicity. Geromedicine 2: 202521, 2026.
37. Laowansiri M, Suwanchote S, Wannigama DL, Badavath VN, Hongsing P, Edwards SW, Suratannon N, Chatchatee P, Lertpichitkul P, Rerknimitr P, *et al*: Monolaurin inhibits antibiotic-resistant Staphylococcus aureus in patients with atopic dermatitis. Sci Rep 15: 23180, 2025.
38. Luo Y, Zhang Z, Zheng W, Zeng Z, Fan L, Zhao Y, Huang Y, Cao S, Yu S and Shen L: Molecular mechanisms of plant extracts in protecting aging blood vessels. Nutrients 16: 2357, 2024.
39. Zheng Y, Pang H, Wang J, Shi G and Huang J: New apoptosis-inducing sesquiterpenoids from the mycelial culture of Chinese edible fungus Pleurotus cystidiosus. J Agric Food Chem 63: 545-551, 2015.
40. Bourrinet P and Quevauviller A: Prosopinine, an alkaloid from Prosopis africana (Legumineous). Its effects on the central and autonomic nervous systems C R Seances Soc Biol Fil 162: 1138-1140, 1968 (In French).
41. Śliwińska S and Jeziorek M: The role of nutrition in Alzheimer's disease. Rocz Panstw Zakl Hig 72: 29-39, 2021.
42. Mammen JSR: Thyroid and aging. Endocrinol Metab Clin North Am 52: 229-243, 2023.
43. Papsdorf K, Miklas JW, Hosseini A, Cabruja M, Morrow CS, Savini M, Yu Y, Silva-García CG, Haseley NR, Murphy LM, *et al*: Lipid droplets and peroxisomes are co-regulated to drive lifespan extension in response to mono-unsaturated fatty acids. Nat Cell Biol 25: 672-684, 2023.
44. Budde J and Skloot GS: Is aging a 'comorbidity' of asthma? Pulm Pharmacol Ther 52: 52-56, 2018.
45. Aslam M and Ladilov Y: Emerging role of cAMP/AMPK signaling. Cells 11: 308, 2022.
46. Quan T: Human skin aging and the anti-aging properties of retinol. Biomolecules 13: 1614, 2023.
47. Rosell-Díaz M, Petit-Gay A, Molas-Prat C, Gallardo-Nuell L, Ramió-Torrentà L, Garre-Olmo J, Pérez-Brocal V, Moya A, Jové M, Pamplona R, *et al*: Metformin-induced changes in the gut microbiome and plasma metabolome are associated with cognition in men. Metabolism 157: 155941, 2024.
48. Hampton K, Polski-Delve A, Hellmich C and Rushworth SA: Linking mitochondria, fatty acids, and hematopoietic stem cell expansion during infection: Implications for aging and metabolic diseases. Stem Cells 43: sxaf053, 2025.
49. Jungwirth H and Kuchler K: Yeast ABC transporters-a tale of sex, stress, drugs and aging. FEBS Let 580: 1131-1138, 2006.

50. Jha NK, Sharma C, Hashiesh HM, Arunachalam S, Meeran MN, Javed H, Patil CR, Goyal SN and Ojha S: β-Caryophyllene, a natural dietary CB2 receptor selective cannabinoid can be a candidate to target the trinity of infection, immunity, and inflammation in COVID-19. Front Pharmacol 12: 590201, 2021.
51. Wu L, He H, Liang T, Du G, Li L, Zhong H, Li Y, Zhang J, Chen N, Jiang T, *et al*: Mesaconic acid as a key metabolite with anti-inflammatory and anti-aging properties produced by Lactobacillus plantarum 124 from centenarian gut microbiota. NPJ Biofilms Microbiomes 11: 165, 2025.
52. Liu R and Sun B: Lactic acid bacteria and aging: Unraveling the interplay for healthy longevity. Aging Dis 15: 1487-1498, 2023.
53. Keshavarz M, Xie K, Schaaf K, Bano D and Ehninger D: Targeting the 'hallmarks of aging' to slow aging and treat age-related disease: Fact or fiction? Mol Psychiatry 28: 242-255, 2023.
54. Kim J, Lee CW, Kim EK, Lee SJ, Park NH, Kim HS, Kim HK, Char K, Jang YP and Kim JW: Inhibition effect of Gynura procumbens extract on UV-B-induced matrix-metalloproteinase expression in human dermal fibroblasts. J Ethnopharmacol 137: 427-433, 2011.
55. Suganuma K, Nakajima H, Ohtsuki M and Imokawa G: Astaxanthin attenuates the UVA-induced up-regulation of matrix-metalloproteinase-1 and skin fibroblast elastase in human dermal fibroblasts. J Dermatol Sci 58: 136-142, 2010.
56. Li J, Sun Z, Cui Y, Qin L, Wu F, Li Y, Du N and Li X: Knockdown of LMNB1 inhibits the proliferation of lung adenocarcinoma cells by inducing DNA damage and cell senescence. Front Oncol 12: 913740, 2022.
57. Ma Y, Wang S, Wang H, Chen X, Shuai Y, Wang H, Mao Y and He F: Mesenchymal stem cells and dental implant osseointegration during aging: From mechanisms to therapy. Stem Cell Res Ther 14: 382, 2023.
58. Mohammad S and Thiemermann C: Role of metabolic endotoxemia in systemic inflammation and potential interventions. Front Immunol 11: 594150, 2021.
59. Zong Z, Xie F, Wang S, Wu X, Zhang Z, Yang B and Zhou F: Alanyl-tRNA synthetase, AARS1, is a lactate sensor and lactyltransferase that lactylates p53 and contributes to tumorigenesis. Cell 187: 2375-2392.e33, 2024.
60. Engeland K: Cell cycle regulation: p53-p21-RB signaling. Cell Death Differ 29: 946-960, 2022.
61. Zhang L, Pan L, Xiang B, Zhu H, Wu Y, Chen M, Guan P, Zou X, Valencia CA, Dong B, *et al*: Potential role of exosome-associated microRNA panels and in vivo environment to predict drug resistance for patients with multiple myeloma. Oncotarget 7: 30876-30891, 2016.
62. Nwabuo CC and Vasan RS: Pathophysiology of hypertensive heart disease: Beyond left ventricular hypertrophy. Curr Hypertens Rep 22: 11, 2020.
63. Dagda RK, Gusdon AM, Pien I, Strack S, Green S, Li C, Van Houten B, Cherra SJ III and Chu CT: Mitochondrially localized PKA reverses mitochondrial pathology and dysfunction in a cellular model of Parkinson's disease. Cell Death Differ 18: 1914-1923, 2011.
64. Signorile A, Ferretta A, Pacelli C, Capitanio N, Tanzarella P, Matrella ML, Valletti A, De Rasmo D and Cocco T: Resveratrol treatment in human parkin-mutant fibroblasts modulates cAMP and calcium homeostasis regulating the expression of mitochondria-associated membranes resident proteins. Biomolecules 11: 1511, 2021.
65. Sanders O and Rajagopal L: Phosphodiesterase inhibitors for Alzheimer's disease: A systematic review of clinical trials and epidemiology with a mechanistic rationale. J Alzheimers Dis Rep 4: 185-215, 2020.
66. Wiciński M, Socha M, Malinowski B, Wódkiewicz E, Walczak M, Górski K, Słupski M and Pawlak-Osińska K: Liraglutide and its neuroprotective properties-focus on possible biochemical mechanisms in Alzheimer's disease and cerebral ischemic events. Int J Mol Sci 20: 1050, 2019.
67. Valenti D, De Rasmo D, Signorile A, Rossi L, de Bari L, Scala I, Granese B, Papa S and Vacca RA: Epigallocatechin-3-gallate prevents oxidative phosphorylation deficit and promotes mitochondrial biogenesis in human cells from subjects with Down's syndrome. Biochim Biophys Acta 1832: 542-552, 2013.
68. Temova Rakuša Ž, Škufca P, Kristl A and Roškar R: Retinoid stability and degradation kinetics in commercial cosmetic products. J Cosmet Dermatol 20: 2350-2358, 2021.
69. Kim J, Lee SG, Lee J, Choi S, Suk J, Lee JH, Yang JH, Yang JS and Kim J: Oral supplementation of low-molecular-weight collagen peptides reduces skin wrinkles and improves biophysical properties of skin: A randomized, double-blinded, placebo-controlled study. J Med Food 25: 1146-1154, 2022.